

ARTICLE

<https://doi.org/10.1038/s41467-019-08806-w>

OPEN

Sleep increases chromosome dynamics to enable reduction of accumulating DNA damage in single neurons

D. Zada¹, I. Bronshtein², T. Lerer-Goldshtein¹, Y. Garini² & L. Appelbaum¹

Sleep is essential to all animals with a nervous system. Nevertheless, the core cellular function of sleep is unknown, and there is no conserved molecular marker to define sleep across phylogeny. Time-lapse imaging of chromosomal markers in single cells of live zebrafish revealed that sleep increases chromosome dynamics in individual neurons but not in two other cell types. Manipulation of sleep, chromosome dynamics, neuronal activity, and DNA double-strand breaks (DSBs) showed that chromosome dynamics are low and the number of DSBs accumulates during wakefulness. In turn, sleep increases chromosome dynamics, which are necessary to reduce the amount of DSBs. These results establish chromosome dynamics as a potential marker to define single sleeping cells, and propose that the restorative function of sleep is nuclear maintenance.

¹The Faculty of Life Sciences and the Multidisciplinary Brain Research Center, Bar-Ilan University, Ramat-Gan 5290002, Israel. ²Department of Physics and the Institute for Nanotechnology, Bar-Ilan University, Ramat-Gan 5290002, Israel. Correspondence and requests for materials should be addressed to L.A. (email: lior.appelbaum@biu.ac.il)

Sleep is vital to animal life and is found in all studied animals, ranging from jellyfish to worm, fly, zebrafish, rodents, and humans^{1–5}. Prolonged sleep deprivation can be lethal, and sleep disturbances are associated with various deficiencies in brain performance⁶. Sleep is regulated by circadian and homeostatic processes⁷, and is coupled with reduced awareness of the environment and a high risk for survival. Several mechanisms can explain the roles of sleep, ranging from macromolecule biosynthesis, energy conservation, and metabolite clearance, to synaptic plasticity and memory consolidation^{8–12}. However, why sleep has evolved and which fundamental ancestral functions it regulates, remain enigmatic.

In mammals and birds, sleep is defined by behavioral criteria and cycles of electroencephalographic (EEG) patterns, which differentiate between wakefulness and sleep states. In non-mammalian animals, including zebrafish, sleep is solely defined by behavioral criteria, such as periods of immobility associated with a species-specific posture and an increased threshold of arousal to external stimuli^{13–16}. In all animals, including animals with simple neuronal networks^{2,3}, circuits of sleep- and wake-promoting neurons orchestrate the behavioral states¹⁷. Evidence across multiple animals supports the notion that sleep can occur locally in the brain¹⁸ or perhaps even in a small number of cells¹⁹. Nevertheless, although sleep significantly contributes to the overall temporal organization of the transcriptome^{20,21}, there are no molecular markers that can be reliably used across phylogeny to define sleep in a single cell²².

The nuclear architecture and the dynamic changes in chromatin organization regulate vital cellular processes, including epigenetics, genomic stability, transcription, cell cycle, and DNA replication and repair^{23,24}. Chromatin dynamics, such as chromosome movements and structural genomic arrangements, are regulated by proteins that interact with the nuclear lamina and envelope in dividing cells^{25–27}. In mature and non-dividing neurons, the role of chromatin dynamics is less understood²⁸. Accumulating evidence showed that chromatin remodeling is implicated in circadian function. The changes in chromatin organization and epigenetic landscape shape the expression profile of a large number of rhythmic genes²⁹. However, the effect of sleep on chromatin dynamics in neurons is unknown.

Recent works showed that sleep can be induced by cellular stress in *Caenorhabditis elegans* and mammals^{30,31}. Moreover, sleep has been associated with the faster repair of DNA double-strand breaks (DSBs) in mice and fruit flies³². The causes of DSBs are diverse and include reactive oxygen species (ROS), ionizing radiation, and inadvertent action of nuclear enzymes³³. Notably, neuronal activity can also induce DSBs. In specific mouse neurons, DSBs can be generated by physiological brain activity during natural exploration of the environment³⁴. Furthermore, activity-induced DSBs facilitate the expression of immediate early genes in mouse and cell cultures, possibly because they resolve topological constraints in the genome³⁵.

We hypothesized that sleep has evolved in order to enable single neurons to perform nuclear maintenance. To test which nuclear process favors sleep time, real-time imaging of chromosome dynamics, neuronal activity as well as quantification of DSBs and sleep, were coupled with genetic and pharmacological manipulations in live zebrafish. The findings propose a definition for a single sleeping neuron; i.e., increased chromosome dynamics, and suggest a role for sleep; i.e., nuclear maintenance.

Results

Imaging chromosome dynamics in live larvae. Chromatin dynamics constitute a fundamental component of genome regulation and cell function³⁶. In order to visualize and quantify

chromosome dynamics in live zebrafish, the zebrafish *telomeric repeat binding factor a* (*terfa*) was cloned, and the telomere marker EGFP-Terfa was expressed in zebrafish neurons, resulting in a nucleus-specific punctum pattern (Fig. 1a–e). To verify that EGFP-Terfa marks chromosomes, the human telomere marker *uas:dsRED-TRF1*³⁷ was co-injected with either *uas:EGFP-Terfa* or the DNA binding-site-deleted construct *uas:EGFP-Terfa del* into one-cell-stage *tg(HuC:Gal4)* embryos. While zebrafish and human telomeric markers co-localized (Fig. 1f–i), deletion of the Terfa DNA binding site resulted in non-specific protein aggregates in the nucleus (Fig. 1j–l). To further validate that the puncta mark chromosomes, the zebrafish *centromere protein a* (*cenpa*) was cloned, and the EGFP-Cenpa was used as a centromere marker. Two-color imaging showed that EGFP-Cenpa and dsRED-TRF1 puncta were expressed adjacently on the chromosome, but not co-localized, as expected from telomeric and centromeric markers (Fig. 1m–p). To continuously image chromosome dynamics in all neurons of live fish, a stable *tg(uas:EGFP-Terfa)* transgenic line was generated and crossed with *tg(HuC:Gal4)* zebrafish (Fig. 1q, r). Neurons in the telencephalon (Te), rhombencephalon (Rh), spinal cord (SC), and habenula (Hb), of 6-day post-fertilization (dpf) larvae were imaged during 9.5 min. Single-particle tracking (SPT) analysis³⁸ was used to detect and quantify the motility of telomere trajectories (Supplementary Movie 1, Fig. 1s, t). While telomeres in the Rh, SC, and Hb neurons showed a similar volume of motion of 0.0069 ± 0.0002 , 0.0066 ± 0.0003 , and $0.0063 \pm 0.0004 \mu\text{m}^3$, respectively, telomeres in Te neurons showed increased volume of motion ($0.01 \pm 0.0004 \mu\text{m}^3$, Supplementary Fig. 1a). Calculation of the mean square displacement (MSD) for single trajectories of all Te and Rh neurons demonstrated anomalous subdiffusion of the puncta (Fig. 1u), which is typical to chromosome diffusion³⁸. Indeed, analysis of both telomeric and centromeric markers that are expressed in the same SC neurons (Fig. 1m–p, Supplementary Movie 2) showed similar dynamics (Supplementary Fig. 1b), verifying that the puncta mark chromosomes. Altogether, these results transfer in vitro chromatin experiments to whole organisms, and demonstrate the capability of monitoring chromosome dynamics in live larvae.

Sleep increases chromosome dynamics in neurons. In the diurnal zebrafish larvae, sleep is regulated by circadian and homeostatic processes and is defined as at least 1 min of immobility accompanied by an increased arousal threshold^{15,39}. Continuous video tracking of behavior showed that, as is the case in WT larvae⁴⁰, 6 dpf *tg(HuC:Gal4)/tg(uas:EGFP-Terfa)* larvae sleep more during the night, under a 14 h light/10 h dark to constant darkness (LD to DD) cycle (day: 8.6 ± 0.7 min/h; night: 28.05 ± 1.2 min/h; subjective day: 17.8 ± 1.01 min/h; Fig. 2a). Moreover, analysis of larval activity specifically during the wake bouts showed that the average time of activity is reduced during the night compared to the day (day: 5.6 ± 0.25 s/min; night: 1.6 ± 0.06 s/min, Supplementary Fig. 2). The behavioral immobility and reduced sensory input during sleep may favor behavioral-state-dependent cellular processes in neurons. Alterations in chromatin structure can affect a variety of nuclear processes, including genome stability, transcription, DNA repair, chromosome segregation, and condensation^{24,37}. To test whether chromosome dynamics change between day and night, single nuclei were imaged in Te and Rh neurons of 6 dpf *tg(HuC:Gal4)/tg(uas:EGFP-Terfa)* larvae during the day [zeitgeber time 4 (ZT4)], night (ZT18), and the following subjective day (ZT4, Fig. 2a). Rh and Te neurons were selected because these regions regulate locomotor activity and cognition, and because these neurons exhibit standard and high levels of chromosome dynamics, respectively (Supplementary Fig. 1a). Remarkably, the time-lapse imaging of

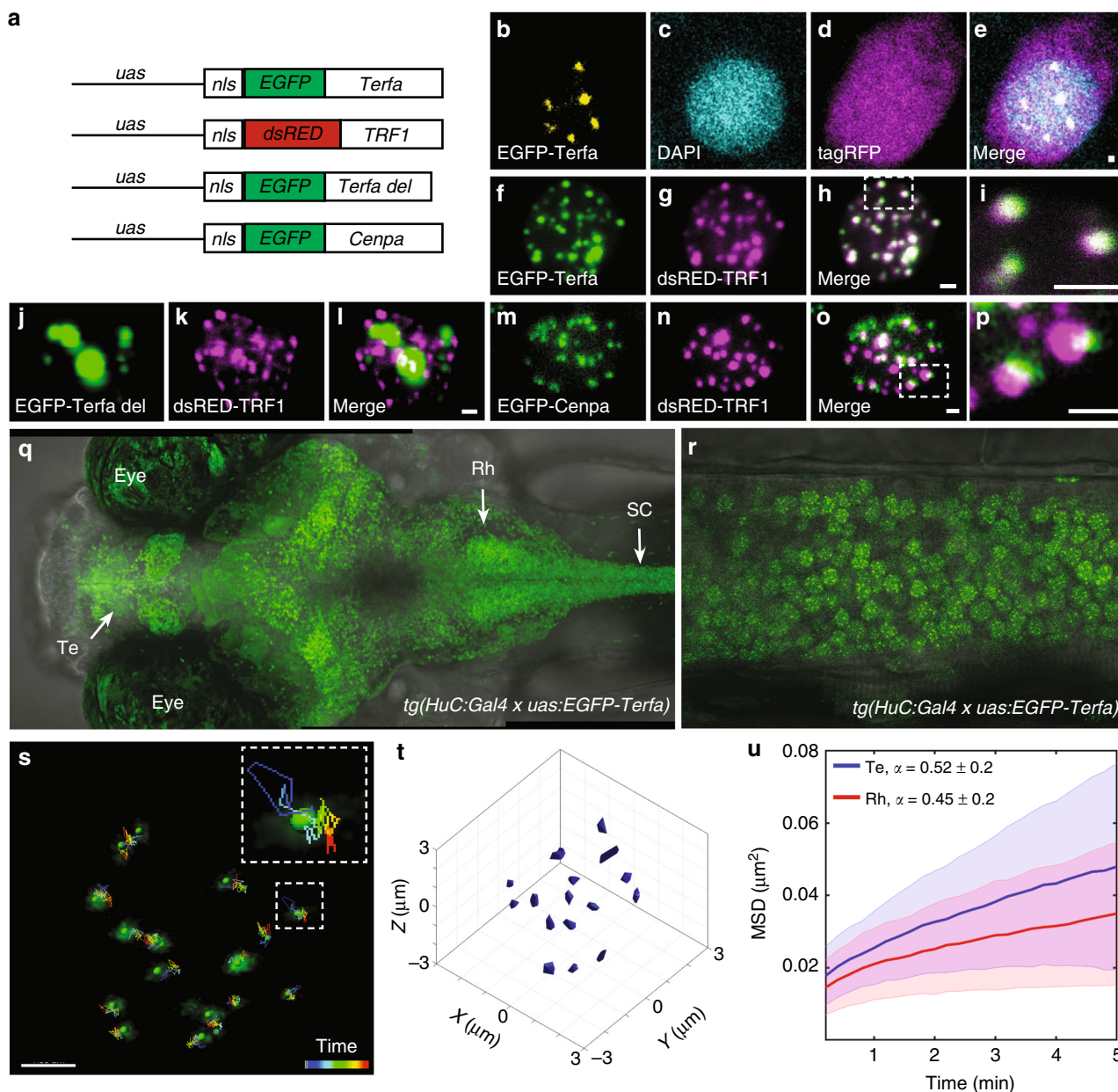


Fig. 1 Imaging single chromosome dynamics in live larvae. **a** The DNA constructs were used to express telomere, centromere, and truncated telomere markers. **b–e** One-plane view of a representative neuron that expresses cellular tagRFP (magenta) and nuclear EGFP-Terfa (yellow) telomeric markers in live larvae. **f–i** Co-localization of zebrafish (**f**) and human (**g**) telomeric markers in the nucleus of a zebrafish neuron. **j–l** Co-expression of truncated zebrafish (**j**) and human (**k**) telomeric markers. **m–p** Co-expression of centromere (**m**) and telomere (**n**) markers. Dorsal (**q**) and lateral (spinal cord, **r**) views of 6-dpf *tg(HuC:Gal4)/tg(uas:EGFP-Terfa)* larvae (Te telencephalon, Rh rhombencephalon, SC spinal cord). **s** Live time-lapse imaging of a single neuron nucleus shows the movement of chromosomes measured over 9.5 min. Dashed box shows high magnification of a single trajectory. **t** 3D single-particle tracking (SPT) shows the volume of motion of chromosomes in a single nucleus. **u** In all Te and Rh neurons, the time-averaged mean square displacement (MSD) for telomeres trajectory (Te: $n = 340$ chromosomes, Rh: $n = 475$ chromosomes). Lines represent the means, and the shaded area represents the standard deviation (SD). Scale bar = $1 \mu\text{m}$

telomere markers showed that chromosome dynamics increased by approximately two-fold during nighttime sleep in both brain regions (average volume of motion, day: Rh— $0.006 \pm 0.0006 \mu\text{m}^3$, Te— $0.01 \pm 0.0008 \mu\text{m}^3$; night: Rh— $0.012 \pm 0.002 \mu\text{m}^3$, Te— $0.023 \pm 0.003 \mu\text{m}^3$; subjective day: Rh— $0.006 \pm 0.0005 \mu\text{m}^3$, Te— $0.011 \pm 0.001 \mu\text{m}^3$, Fig. 2b–e, Supplementary Movie 3, 4). Using centromeric markers, similar changes in chromosome dynamics were visualized in SC neurons (day: $0.0047 \pm 0.0004 \mu\text{m}^3$; night: $0.0078 \pm 0.0006 \mu\text{m}^3$, Fig. 2f, Supplementary Movie 2). In order to differentiate between sleep and circadian effect, the 6 dpf *tg(HuC:*

Gal4)/tg(uas:EGFP-Terfa) larvae were sleep-deprived for 4 h during the night, and behavioral sleep rebound was observed during the following subjective day (ZT4; LD to DD: 12.4 ± 0.8 min/h; SD: 27.5 ± 1.3 min/h, Fig. 2a). Immediately following SD, chromosome dynamics were reduced by approximately two-fold (Rh— $0.0062 \pm 0.0005 \mu\text{m}^3$, Te— $0.01 \pm 0.0009 \mu\text{m}^3$, Fig. 2d, e) compared with the levels observed during the night in the control group, and were similar to the levels observed during the day. On the following day, after 10 h of recovery, when the sleep-deprived larvae demonstrated sleep rebound (Fig. 2a), chromosome

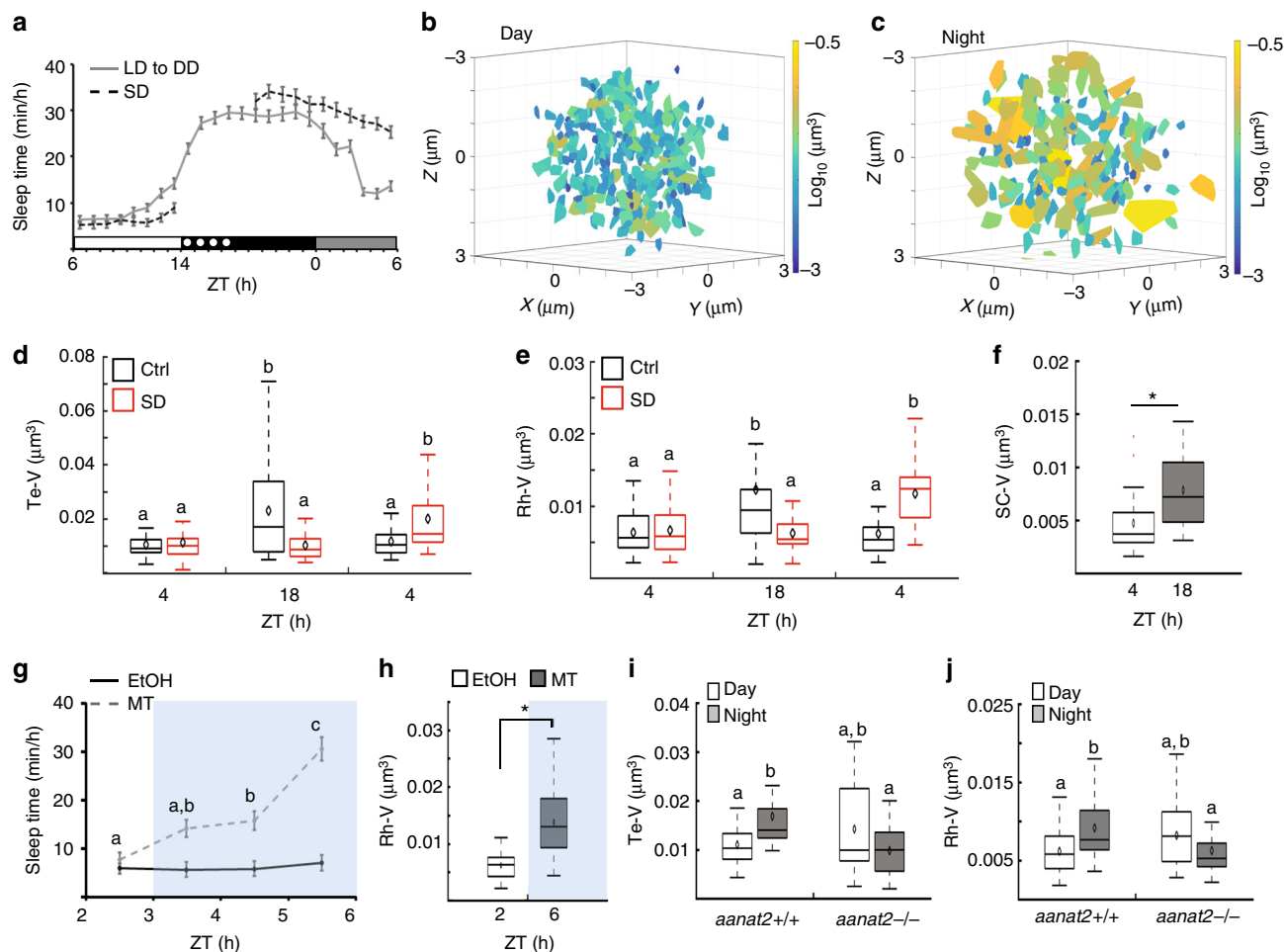


Fig. 2 Sleep increases chromosome dynamics in neurons. **a** Recording of sleep was performed in 6 dpf control or sleep-deprived larvae under an 14 h light/10 h dark cycle following by constant darkness (LD to DD, control: $n = 119$ larvae, sleep deprivation (SD): $n = 96$ larvae). **b, c** The area scanned by all chromosomes from all imaged Te neurons during 9.5 min (day: $n = 26$ cells; night: $n = 29$ cells). Color was coded according to the levels of volume of motion. **d-f** Volume of chromosome dynamics over 9.5 min per cell (EGFP-Terfa in **d** and **e**, EGFP-Cenpa in **f**). **d** Te neurons, ctrl: day ($n = 26$ cells), night ($n = 29$ cells), subjective day ($n = 25$ cells). SD: day ($n = 26$ cells), night ($n = 35$ cells), subjective day ($n = 25$ cells). $P = 1.3 \times 10^{-7}$, $F = 17.54$, degrees of freedom = 2. **e** Rh neurons, ctrl: day ($n = 23$ cells), night ($n = 30$ cells), subjective day ($n = 35$ cells). SD: day ($n = 27$ cells), night ($n = 25$ cells), subjective day ($n = 26$ cells). $P = 7 \times 10^{-6}$, $F = 12.82$, degrees of freedom = 2, determined by two-way ANOVA followed by Tukey test. **f** SC neurons: day ($n = 33$ cells), night ($n = 33$ cells). $*P = 0.0001$, determined by two-tailed t -test: two samples assuming unequal variance. Red crosses indicate outliers. **g, h** Monitoring sleep and chromosome dynamics under melatonin (MT) treatment. Blue background represents time under treatment. **g** Pretreated and EtOH/MT-treated larvae (EtOH: $n = 48$; MT: $n = 48$ larvae). $P = 7.4 \times 10^{-4}$, $F = 14.3$, degrees of freedom = 3, determined by two-way ANOVA followed by Tukey test. Values are presented as means \pm SEM. **h** Pre-treated cells ($n = 22$) and MT-treated cells ($n = 25$). $*P = 7 \times 10^{-6}$, determined by two-tailed t -test: two samples assuming unequal variance. **i** Te neurons, *aanat2*^{+/+}: day ($n = 16$ cells), night ($n = 21$ cells). *aanat2*^{-/-}: day ($n = 14$ cells), night ($n = 32$ cells). $P = 1.7 \times 10^{-3}$, $F = 12.26$, degrees of freedom = 1. **j** Rh neurons, *aanat2*^{+/+}: day ($n = 24$ cells), night ($n = 24$ cells). *aanat2*^{-/-}: day ($n = 19$ cells), night ($n = 30$ cells). $P = 7.6 \times 10^{-4}$, $F = 10.42$, degrees of freedom = 1, determined by two-way ANOVA followed by Tukey test. Boxplots: black diamond represents the mean, boxes indicate the median and the 25th-to-75th percentiles, whiskers extend to the most extreme data points. Letters or asterisks indicate significant differences. ZT zeitgeber time

dynamics increased by approximately two-fold (Rh— $0.011 \pm 0.0008 \mu\text{m}^3$, Te— $0.02 \pm 0.002 \mu\text{m}^3$, Fig. 2d, e) in the sleep-deprived larvae, and reached the levels observed during nighttime sleep in the sibling control larvae. These results show that sleep increases chromosome dynamics in a homeostatic-dependent manner.

To further validate the regulation of chromosome dynamics by the sleep state, the *tg(HuC:Gal4)/tg(uas:EGFP-Terfa)* larvae were treated during the day with melatonin, which is a strong sleep-promoting hormone in the diurnal zebrafish^{14,41}. Sleep time and chromosome dynamics were monitored prior to and during melatonin treatment. As expected, while ethanol (EtOH) administration did not affect sleep time, under 3 h of melatonin

treatment, sleep increased in melatonin-treated larvae (prior to melatonin treatment: 7.7 ± 1.5 min/h; 3 h following melatonin treatment: 30.7 ± 2.4 min/h, Fig. 2g). In accordance, melatonin-derived sleep increases chromosome dynamics (prior to melatonin treatment: $0.006 \pm 0.0005 \mu\text{m}^3$; during melatonin treatment: $0.013 \pm 0.0013 \mu\text{m}^3$, Fig. 2h). Thus, sleep is sufficient to increase chromosome dynamics. In order to understand if sleep is not only sufficient but also necessary to increase chromosome dynamics, we crossed the *tg(HuC:Gal4)/tg(uas:EGFP-Terfa)* zebrafish with arylalkylamine N-acetyltransferase-2⁴² mutant zebrafish (*aanat2*^{-/-}), which lack melatonin signaling. The *aanat2*^{-/-} larvae exhibit reduced sleep time during the night, although their intrinsic molecular circadian clock is intact⁴³. Imaging single

neurons during day and night revealed that while chromosome dynamics increased in *aanat2*^{+/+} larvae during the night (day: Rh— $0.006 \pm 0.0006 \mu\text{m}^3$, Te— $0.01 \pm 0.001 \mu\text{m}^3$; night: Rh— $0.009 \pm 0.0009 \mu\text{m}^3$, Te— $0.014 \pm 0.0008 \mu\text{m}^3$, Fig. 2i, j), as was the case in WT larvae (Fig. 2d, e), it was reduced during the night in *aanat2*^{-/-} (night: Rh— $0.006 \pm 0.0006 \mu\text{m}^3$, Te— $0.009 \pm 0.0009 \mu\text{m}^3$) compared with *aanat2*^{+/+} larvae. Thus, although the molecular circadian clock is intact, chromosome dynamics were similar in both day and night, which is in accordance with the reduced nighttime sleep in *aanat2*^{-/-} larvae (Fig. 2i, j). These results show that chromosome dynamics in neurons are regulated by the behavioral sleep/wake state.

Sleep-dependent changes in chromosome dynamics may not be specific to neurons. To test whether these changes are also present in other cell types, we monitored chromosome dynamics in peripheral endothelial and Schwann cells. Chromosome dynamics were imaged during day and night in endothelial and Schwann cells using *tg(fli:Gal4)/tg(uas:EGFP-Terfa)* and *mbp:Gal4*-injected *tg(uas:EGFP-Terfa)* 6 dpf larvae, respectively (Supplementary Fig. 3a, b). Chromosome dynamics did not differ between day and night in both cell types (Supplementary Fig. 3c). These results show that sleep-dependent changes in chromosome dynamics that were observed in neurons, do not occur in endothelial or Schwann cells.

Sleep reduces DSBs that are accumulated during wakefulness.

What is the physiological benefit of sleep-dependent chromosome dynamics? Since the genome can be hit by dozens of DSBs per day^{33,44}, we speculated that sleep and increased chromosome dynamics are essential for the recovery from wakefulness-derived DNA damage. To test our hypothesis, the levels of DSBs and chromosome dynamics were monitored in Rh neurons during the 24-h sleep/wake cycle. The γH2AX marker, which is activated as part of the DNA damage response system⁴⁵, was used to quantify DSBs during day and night in single cells (Fig. 3a–e). Whole head staining showed increased localization of γH2AX in the Te compared to other brain areas, such as the Rh (Fig. 3a). This DSB enrichment is correlated with the increased neuronal activity detected in the Te (Supplementary Fig. 4). In the 24-h experiment, we quantified DSBs in the Rh because it better represents the distribution of γH2AX in the entire CNS. During the day, the number of DSBs consistently increased, and peaked 1 h before darkness ($15.1 \pm 0.46 \gamma\text{H2AX}$ foci, Fig. 3d). During the night, the number of DSBs dramatically decreased, reached the minimum levels at ZT19 ($5.4 \pm 0.24 \gamma\text{H2AX}$ foci, Fig. 3d), and remained low until the beginning of the day. Concurrently, during the day, chromosome dynamics remained at similar low levels (ZT1: 0.0063 ± 0.0007 ; ZT5: 0.0067 ± 0.0005 ; ZT9: 0.007 ± 0.0008 ; ZT13: $0.0065 \pm 0.0005 \mu\text{m}^3$, Fig. 3d). In contrast, following 1 h of darkness, chromosome dynamics increased by two-fold, and the high levels were maintained during the entire night (ZT15: 0.014 ± 0.0016 ; ZT19: 0.012 ± 0.0018 ; ZT23: $0.01 \pm 0.0011 \mu\text{m}^3$, Fig. 3d). These results show that while chromosome dynamics keep constant low levels, DSB number accumulates during the day. During the night, following robust increase in chromosome dynamics, the number of DSBs was gradually reduced, showing that chromosome dynamics correlate with efficient reduction of DSBs during the night.

In order to distinguish between circadian and sleep effect on DSB levels, we quantified the number of DSBs in sleep-deprived larvae. In the control group, the number of γH2AX foci per cell in the Rh neurons decreased during the night and increased back to daytime levels on the following subjective day (day: 9.3 ± 0.61 ; night: 6.1 ± 0.36 , subjective day: 10.16 ± 0.46 , Fig. 3e). In contrast, following SD, the γH2AX foci number increased during the night

(11.9 ± 0.37), and then, post-sleep recovery, was reduced on the following subjective day (6.76 ± 0.44 , Fig. 3e). These experiments show that DSBs increased during wakefulness and decreased during sleep in neurons.

In order to test whether the amount of DSBs changed between day and night in other cell types, we performed immunostaining assays using both anti- γH2AX and anti-EGFP in *tg(fli:EGFP)* and *tg(mbp:EGFP)* 6 dpf larvae (Supplementary Fig. 3d–i). In contrast to the day/night changes observed in neurons, the number of DSBs was constantly low during day and night in endothelial and Schwann cells (Supplementary Fig. 3j), suggesting that wakefulness and sleep do not affect the levels of DSBs in these cells.

Chromosome dynamics are necessary to reduce DSBs. In order to causally link chromosome dynamics and the efficient reduction in DNA damage, we manipulated chromosome dynamics by overexpressing the zebrafish Lamina-associated polypeptide 2 (Lap2 β) in specific neurons. This protein physically interacts with lamins and anchors chromatin to the nuclear lamina in mammals and zebrafish^{46,47}. In order to monitor chromosome dynamics and DSBs in Lap2 β -overexpressing and control neurons, *pT2-uas:Lap2 β -EGFP* and *pT2-uas:dsRED-TRF1* constructs were co-injected into *tg(HuC:Gal4)* embryos, and neurons that express either both Lap2 β -EGFP and dsRED-TRF1 (Fig. 3f–h) or only dsRED-TRF1 in the SC were analyzed during day and night in 6 dpf larvae. As expected, chromosome dynamics increased during the night in the control dsRED-TRF1-expressing neurons (day: 0.006 ± 0.0004 ; night: $0.009 \pm 0.001 \mu\text{m}^3$, Fig. 3i). In contrast, overexpression of Lap2 β inhibited chromosome dynamics, specifically during the night, and the levels were similar during both day and night (day: 0.005 ± 0.0005 ; night: $0.005 \pm 0.0007 \mu\text{m}^3$, Fig. 3i). Thus, the overexpression of Lap2 β impedes the sleep-dependent increase of chromosome dynamics. Next, we measured the number of γH2AX foci in the control and in Lap2 β -overexpressing neurons. As was found in the Rh (Fig. 3b–e), the number of γH2AX foci per neuron in the SC decreased by approximately 30% during the night (day: 5.1 ± 0.18 ; night: 3.5 ± 0.14 , Fig. 3j, k, m). Remarkably, the number of γH2AX foci increased by 120% in Lap2 β -overexpressing neurons compared with the control neurons during the night ($7.95 \pm 0.63 \gamma\text{H2AX}$ foci, Fig. 3l, m). These results show that genetic inhibition of chromosome dynamics increases the number of DSBs specifically during nighttime sleep. Furthermore, these results suggest that sleep-dependent increase in chromosome dynamics is necessary to reduce DNA damage.

Neuronal activity can reduce chromosome dynamics. Which cellular processes induce DSBs during wakefulness, and how do they affect chromosome dynamics? In mammals, neuronal activity promotes the formation of DSBs^{34,35}. In zebrafish, we found sleep-dependent changes in the levels of chromosome dynamics and DSBs in neurons (Figs. 2 and 3) but not in two other non-excitabile cell types (Supplementary Fig. 3), and showed correlation between increased spontaneous neuronal activity and enriched expression of γH2AX in the Te (Fig. 3a, Supplementary Fig. 4). Therefore, since chromosome dynamics is required to reduce the number of DSBs we rationalized that the intensity and frequency of neuronal activity should affect chromosome dynamics within individual neurons. To study activity-dependent chromosome dynamics, a *tg(uas:RCaMP1b)* transgenic fish was generated and crossed with the *tg(HuC:Gal4)/tg(uas:EGFP-Terfa)* line. Then, spontaneous chromosome dynamics and neuronal activity were simultaneously imaged in one plane in single neurons within the Rh during day and night (Fig. 4a–c). The results showed moderate negative correlation between neuronal activity

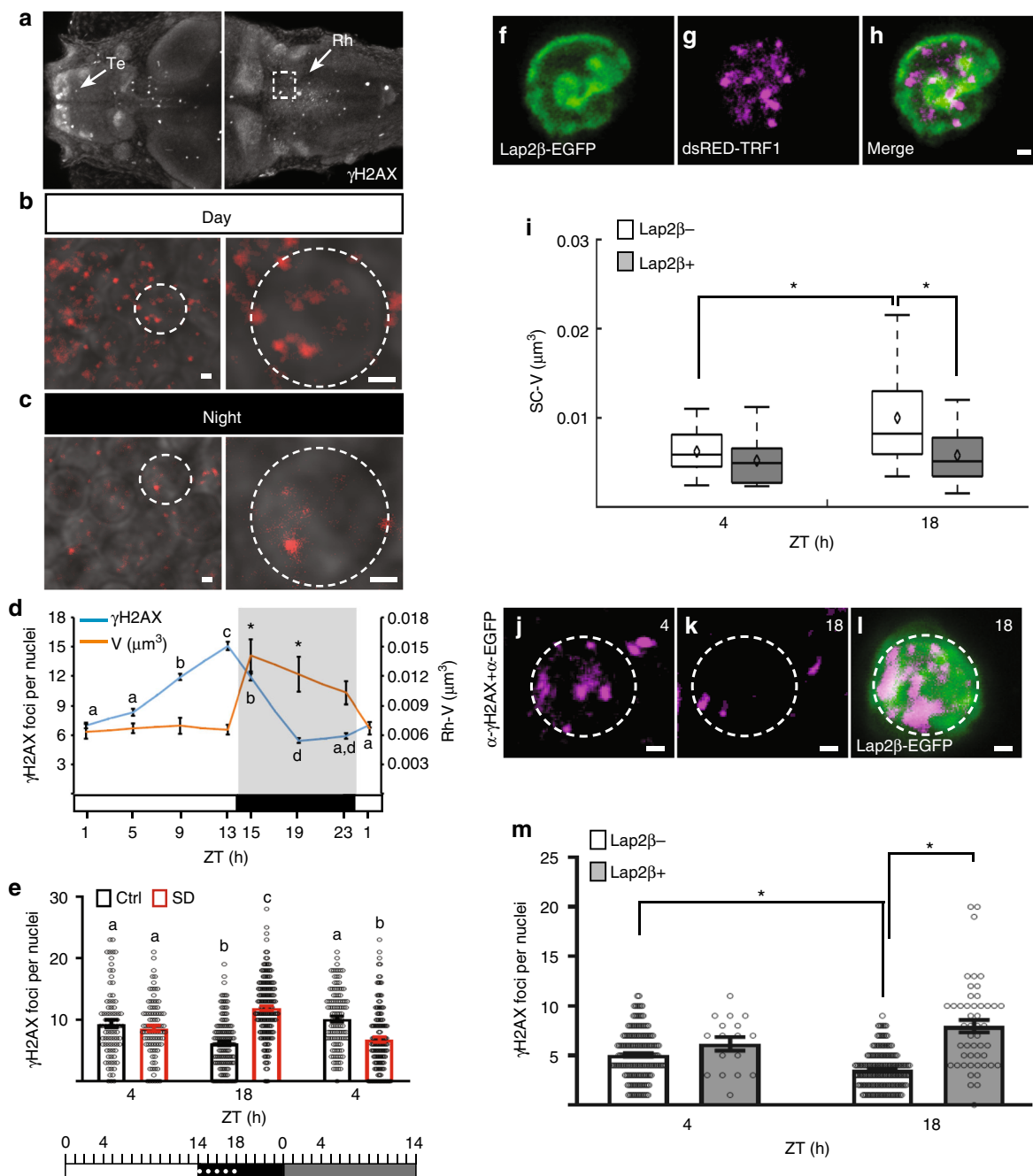


Fig. 3 Chromosome dynamics are essential for reducing the number of accumulating DSBs. **a–c** Dorsal view of 6 dpf larvae stained with γ H2AX. **a** Arrows indicate the telencephalon (Te) and rhombencephalon (Rh). Dashed box showing the Rh represents the area analyzed in **d** and **e**. Representative images from the Rh region during day (**b**) and night (**c**) are shown. Dashed circle indicates a single neuron. **d** The number of DSBs ($P = 1 \times 10^{-16}$, $F = 118$, degrees of freedom = 7) and chromosome dynamics ($*P = 8 \times 10^{-7}$, $F = 7$, degrees of freedom = 7) in single nuclei over 24 h, in 14 h light/10 h dark cycle. Determined by one-way ANOVA followed by a Tukey test. Lower case letters indicate significant changes over γ H2AX groups. Asterisks indicate significant changes between chromosome dynamics groups. White and black horizontal bars represent light and dark periods, respectively. **e** Numbers of DSBs (dot plot, means \pm SEM). Ctrl: day ($n = 83$ cells), night ($n = 131$ cells), subjective day ($n = 105$ cells). SD: day ($n = 86$ cells), night ($n = 170$ cells), subjective day ($n = 135$ cells). $P = 1 \times 10^{-6}$, $F = 62.04$, degrees of freedom = 2, determined by two-way ANOVA followed by a Tukey test. White, black, and gray rectangles represent day, night, and subjective day, respectively. Dotted white line represents the sleep deprivation (SD) period. **f–h** Co-expression of Lap2 β -EGFP (**f**) and human telomeric markers (**g**) in SC-neuronal nuclei. **i** Volume of chromosome dynamics in control (Lap2 β^{-} , day: $n = 25$; night: $n = 21$ cells) and Lap2 β -overexpressing cells (Lap2 β^{+} , day: $n = 25$; night: $n = 19$ cells). $*P = 0.026$, $F = 5.1$, degrees of freedom = 1, determined by two-way ANOVA followed by a Tukey test. **j–l** Representative images of double immunohistochemistry using α - γ H2AX (magenta) and α -EGFP (green) in single SC neurons during day (**j**) and night (**k**, **l**). Dashed circle indicates a single nucleus. **m** The number of DSBs (dot plot, means \pm SEM) in control (Lap2 β^{-} , day: $n = 177$; night: $n = 177$ cells) and Lap2 β -overexpressing cells (Lap2 β^{+} , day: $n = 17$; night: $n = 49$ cells). $*P = 1 \times 10^{-6}$, $F = 18.8$, degrees of freedom = 1, determined by two-way ANOVA followed by a Tukey test. Zeitgeber time (ZT4)-day, ZT18-night. Boxplots: black diamond represents the mean, boxes indicate the median and the 25th-to-75th percentiles, whiskers extend to the most extreme data points. Letters or asterisks indicate significant differences. Scale bar = 1 μ m

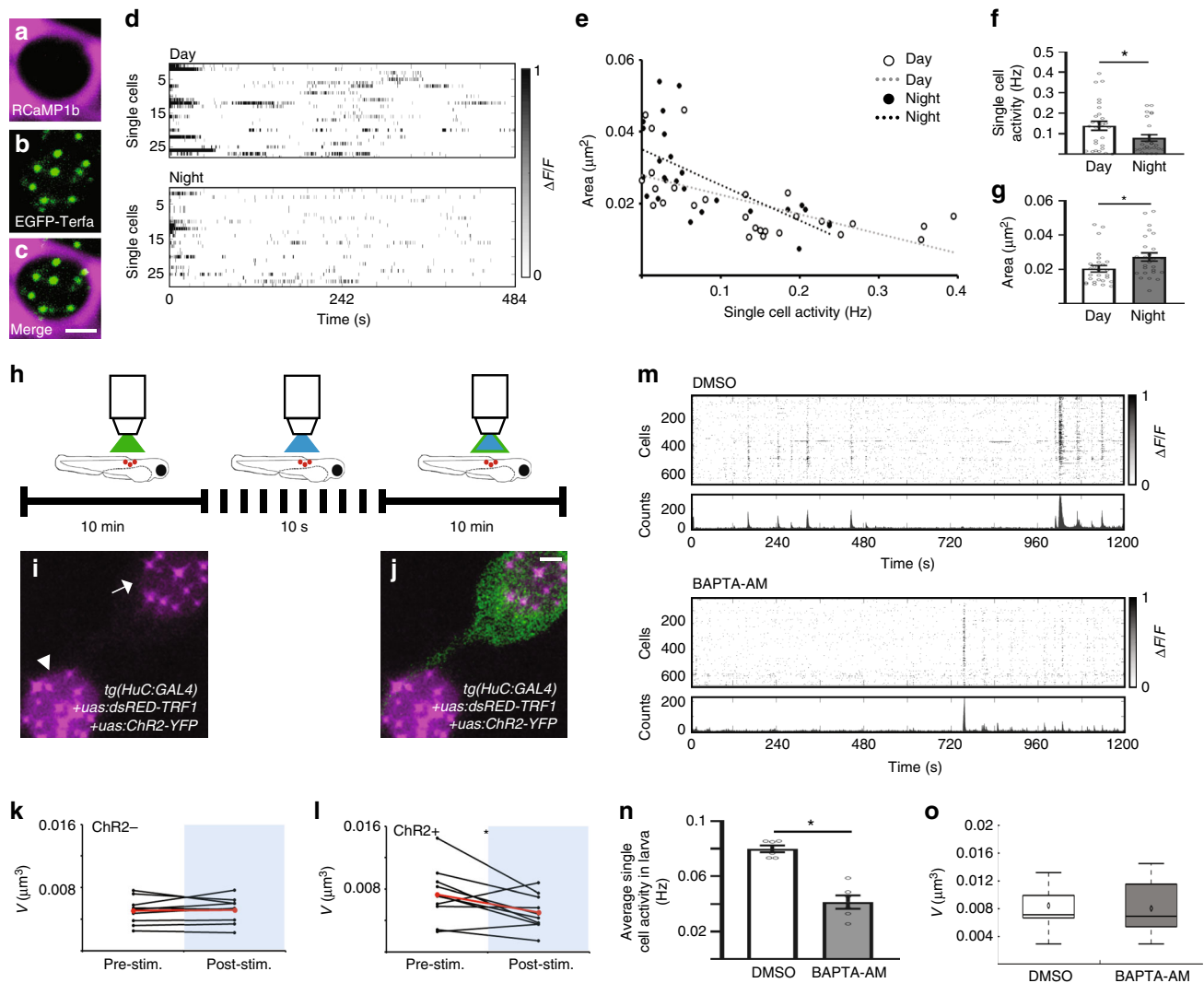


Fig. 4 Neuronal excitation reduces chromosome dynamics in the Rh and SC. **a–c** Simultaneous 2D imaging of neuronal activity (magenta) and chromosome dynamics (green) in the Rh neurons. **d** Raster plot of $\Delta F/F$ of 27 and 26 RCaMP1b-expressing single cells during day and night, respectively. Grayscale: $\Delta F/F$ amplitude. **e** A moderate negative correlation between chromosome dynamics and neuronal activity during day and night ($R_{\text{Day}} = -0.62$, $R_{\text{Night}} = -0.64$, $R_{\text{Total}} = -0.64$), determined by Pearson correlation coefficient. The average single-cell activity (**f**, $*P_{\text{activity}} = 0.035$) and chromosome dynamics (**g**, $*P_{\text{dynamics}} = 0.03$) during day and night. Determined by two-tailed *t*-test: two samples assuming unequal variance. **h–j** Optogenetic stimulation of neuronal activity reduces chromosome dynamics. **h–j** The neurons expressed both dsRED-TRF1 and ChR2-YFP (arrow) or only dsRED-TRF1 (arrowhead). **k, l** Chromosome dynamics before and following the light stimuli (ChR2⁻, $n = 9$ cells; ChR2⁺, $n = 10$ cells). $*P = 0.031$, determined by two-tailed *t*-test: two-paired samples for means. Average change is marked by red line. **m–o** Inhibition of neuronal activity during the night does not affect chromosome dynamics. **m** Representative raster plots of $\Delta F/F$ in the Rh of 6 dpf *tg(HuC:GCaMP5)* larvae under DMSO ($n = 6$ larvae) or BAPTA-AM ($n = 6$ larvae) treatments. Grayscale: $\Delta F/F$ amplitude. Bottom: histogram of the Ca^{2+} transients of all cells. **n** Average spontaneous neuronal activity in single neurons of the Rh under either DMSO ($n = 6$ larvae) or BAPTA-AM ($n = 6$ larvae) treatment (ZT23). $*P = 2 \times 10^{-4}$, $t = 2.3$, degrees of freedom = 7, determined by two-tailed *t*-test: two samples assuming unequal variance. **o** Volume of chromosome dynamics during nighttime (ZT23) in DMSO ($n = 13$ cells) and BAPTA-AM ($n = 11$ cells)-treated larvae. Values are presented as boxplots and means (black diamonds) or as dot plots and means \pm SEM. Boxplots indicate the median and the 25th-to-75th percentiles. The whiskers extend to the most extreme data points. ZT zeitgeber time. Scale bar = $2 \mu\text{m}$

and chromosome dynamics (Fig. 4d–g). While the average frequency of single cell activity was reduced (day: 0.138 ± 0.022 Hz; night: 0.079 ± 0.015 Hz, Fig. 4d–f), the average chromosome dynamics increased during the night in Rh neurons (day: $0.02 \pm 0.002 \mu\text{m}^2$; night: $0.027 \pm 0.002 \mu\text{m}^2$, Fig. 4e, g). Taking into account that neurons in the Rh and SC regulate tail movement and locomotor activity⁴⁸, which are markedly reduced during sleep, these results show that, at the single-cell level, chromosome dynamics increased in resting cells during the night.

In order to causally test the effect of neuronal activity on chromosome dynamics, we used optogenetics and transiently

expressed the neural-activating cation channel channelrhodopsin-2 (ChR2-YFP)⁴⁹ and the telomere marker dsRED-TRF1 in neurons of the SC (Fig. 4h–j), which showed similar chromosome dynamics and spontaneous neuronal activity as in Rh neurons (Supplementary Fig. 1a, Supplementary Fig. 4). Chromosome dynamics were quantified in single cells that did or did not express the ChR2-YFP before and following blue light stimulation during daytime wakefulness (Fig. 4h–j). While chromosome dynamics did not change post-stimulation in dsRED-TRF1-expressing cells (Fig. 4k), they were reduced in stimulated dsRED-TRF1+ChR2-YFP-expressing cells (pre-stimulation: $0.0073 \pm 0.001 \mu\text{m}^3$;

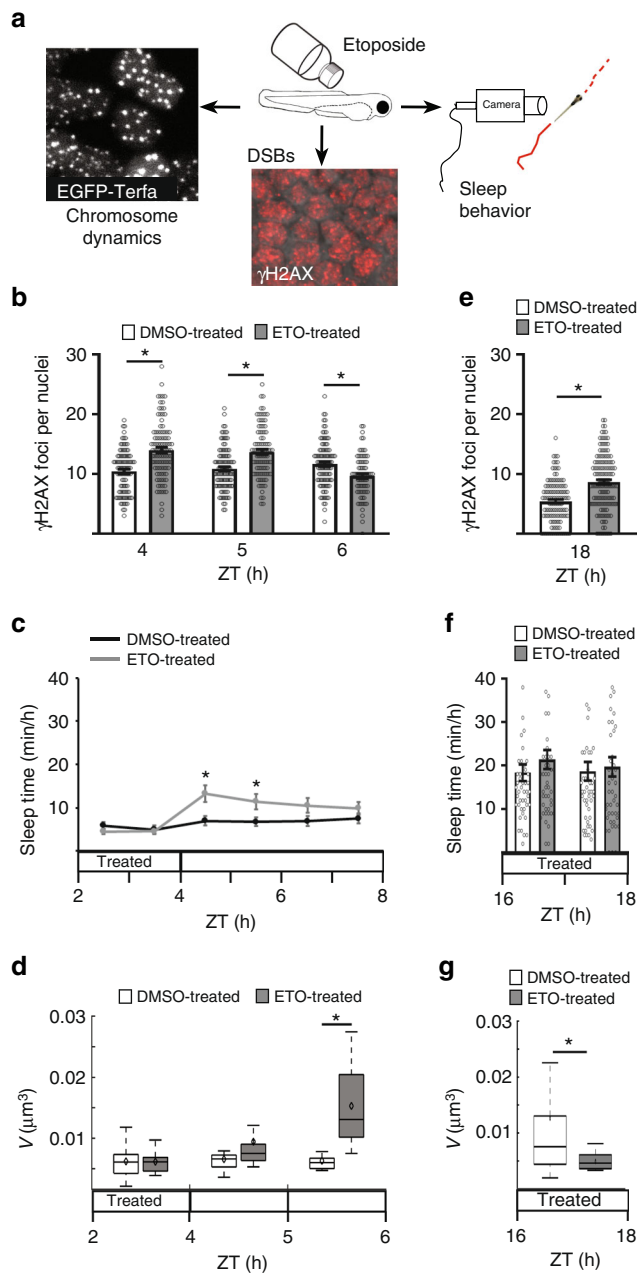


Fig. 5 Sleep and chromosome dynamics increased following induction of DSBs. **a** Larvae were treated with etoposide (ETO) during the day (ZT2–4, **b–d**) and night (ZT16–18, **e–g**), and DSBs, chromosome dynamics, and sleep were quantified. **b** Number of γ H2AX foci in single nuclei. During treatment (DMSO: $n = 93$ cells; ETO: $n = 99$ cells, $*P = 2.2 \times 10^{-8}$), 1 h following treatment (DMSO: $n = 102$ cells; ETO: $n = 89$ cells, $*P = 2.2 \times 10^{-6}$), 2 h following treatment (DMSO: $n = 98$ cells; ETO: $n = 73$ cells, $*P = 6.8 \times 10^{-4}$). **c** Total sleep time. DMSO-treated ($n = 84$ larvae), ETO-treated ($n = 78$ larvae), $P_{ZT2-3} = 0.18$, $P_{ZT3-4} = 0.71$. Post-treatment: DMSO-treated ($n = 84$ larvae), ETO-treated ($n = 78$ larvae), $*P_{ZT4-5} = 0.0035$, $*P_{ZT5-6} = 0.02$, $P_{ZT6-7} = 0.07$, $P_{ZT7-8} = 0.2$. **d** Chromosome dynamics in neurons. During treatment (DMSO: $n = 22$ cells; ETO: $n = 11$ cells), 1 h following treatment (DMSO: $n = 17$ cells; ETO: $n = 13$ cells), 2 h following treatment (DMSO: $n = 11$ cells; ETO: $n = 16$ cells, $*P = 3.8 \times 10^{-5}$). Red crosses indicate outliers. **e–g** Number of γ H2AX foci in single neuronal nuclei (**e**, DMSO: $n = 118$; ETO: $n = 138$ cells, $*P = 1.65 \times 10^{-9}$), total sleep time (**f**, DMSO: $n = 48$; ETO: $n = 48$ larvae), and chromosome dynamics (**g**, DMSO: $n = 22$; ETO: $n = 14$ cells, $*P = 0.02$) in DMSO- and ETO-treated larvae during the night. Significant differences of all experiments were determined by two-tailed t -test: two samples assuming unequal variance. Values are presented as boxplots and means (black diamonds) or as dot plots and means \pm SEM. Boxplots indicate the median and the 25th-to-75th percentiles. The whiskers extend to the most extreme data points. ZT zeitgeber time. Scale bar = $1 \mu\text{m}$.

AM— $0.008 \pm 0.001 \mu\text{m}^3$, Fig. 4o). These results indicate that neuronal activity is not an essential regulator of chromosome dynamics; however, it can reduce chromosome dynamics, possibly via the induction of DSBs.

Sleep and chromosome dynamics increased following induction of DSBs. Neuronal activity is only one of several processes that can induce DSBs during wakefulness. The causes for DNA damage are diverse and include intrinsic and extrinsic factors³³. In order to simulate the effect of these different factors, we used etoposide (ETO), which induces DSBs⁴⁵, and the number of γ H2AX foci, chromosome dynamics, and sleep time were monitored during the day (Fig. 5a–d). As expected, after 2 h under ETO treatment (ZT2–4), the γ H2AX foci number increased (DMSO: 10.44 ± 0.37 ; ETO: 14.01 ± 0.47 , Fig. 5b). Furthermore, sleep time (Fig. 5c) and chromosome dynamics (Fig. 5d) did not change under ETO treatment. However, 1 h following ETO withdrawal, sleep time increased in ETO-treated larvae (DMSO: 6.95 ± 1.1 min/h; ETO: 13.28 ± 1.8 min/h, Fig. 5c), while DSB levels remained high (DMSO: 10.87 ± 0.35 ; ETO: 13.7 ± 0.46 γ H2AX foci, Fig. 5b) and chromosome dynamics remained low (DMSO: 0.0065 ± 0.0004 ; ETO: $0.0094 \pm 0.001 \mu\text{m}^3$, Fig. 5d). Notably, following 2 h of recovery from the ETO treatment, sleep time remained high (DMSO: 6.71 ± 1 min/h; ETO: 11.4 ± 1.8 min/h, Fig. 5c), and chromosome dynamics increased by approximately two-fold (DMSO: 0.0062 ± 0.0005 ; ETO: $0.015 \pm 0.0017 \mu\text{m}^3$, Fig. 5d), accompanied by a reduction of the number of DSBs (9.65 ± 0.42 γ H2AX foci, Fig. 5b). In order to examine how the formation of DSBs will affect sleep time and chromosome dynamics during the night, we exposed the larvae to ETO for 2 h (ZT16–18). Similar to the results obtained during the day, under ETO treatment, the γ H2AX foci number increased by 60% (DMSO: 5.4 ± 0.33 ; ETO: 8.66 ± 0.4 , Fig. 5e) and sleep time did not change (Fig. 5f). However, chromosome dynamics decreased by approximately two-fold (DMSO: 0.0126 ± 0.003 ; ETO: $0.0049 \pm 0.0004 \mu\text{m}^3$, Fig. 5g). These results suggest that while chromosome dynamics are low during the formation of DSBs, the accumulation of DSBs during wakefulness triggers sleep, which increases chromosome dynamics and eventually reduces the number of DSBs.

post-stimulation: $0.005 \pm 0.0007 \mu\text{m}^3$, Fig. 4l). Thus, neuronal activity reduces chromosome dynamics in a single active cell under spontaneous conditions and optogenetic manipulation.

Neuronal activity could affect chromosome dynamics via the formation of DSBs. In order to uncouple neuronal activity from DNA damage, neuronal activity was inhibited specifically during the night, when the DSB level is low. The Ca^{+2} chelator BAPTA-AM, which lowers intracellular Ca^{+2} levels, was used. To validate the efficiency of BAPTA-AM in Rh neurons, we quantified spontaneous neuronal activity in BAPTA-AM-treated and control 6 dpf *tg(HuC: GCaMP5)* larvae. As expected, the average activity of a single Rh neuron was reduced by two-fold in BAPTA-AM-treated larvae compared with the control group (DMSO: 0.08 ± 0.002 Hz; BAPTA-AM: 0.04 ± 0.004 Hz, Fig. 4m, n). In these neurons, chromosome dynamics were monitored at the end of the night (ZT23), when the DNA damage is low (Fig. 3d). Inhibition of neuronal activity did not affect chromosome dynamics, which remain high in both BAPTA-AM-treated and control larvae (DMSO— 0.0084 ± 0.001 , BAPTA-

Discussion

The beneficial role of sleep in simple neuronal networks and in the complex brain is a mystery^{50,51}, and it is unclear if and why a single neuron requires sleep. The methods developed in this work enable the study of sleep-dependent nuclear processes in single cells of live animals. We visualized 3D motions of individual chromosomes, DSBs, neuronal activity and behavior in live zebrafish, and directly linked the physiology of single neurons to the entire organism during sleep and wakefulness. Genetic and pharmacological manipulation of the melatonin signaling, as well as SD experiments, revealed that chromosome dynamics increased about two-fold during sleep in neurons. These sleep-dependent changes were not observed in two other non-excitable cell types. In neurons, DSBs accumulate during wakefulness and SD, when chromosome dynamics are low. Imaging of spontaneous neuronal activity, single-cell optogenetic and pharmacological experiments indicated that DSB formation by neuronal activity and other factors, can reduce chromosome dynamics. In turn, sleep benefits the brain because it increases chromosome dynamics, which are essential for the efficient reduction of the number of DSBs (Fig. 6).

Why do chromosome dynamics increase during sleep? The dynamic organization of the genome is often altered in diseases⁵², and changes in chromatin dynamics have been shown to regulate key nuclear processes, including epigenetics, DNA damage and repair, transcription, and enhancer–promoter interaction. For example, transcriptional activation by enhancers and promoters is associated with an increase in their loci mobility in live embryonic stem cells⁵³. However, although across the sleep–wake cycle global gene expression in the brain is dynamically regulated, the expression of the majority of genes peaks during wakefulness^{9,54}, whereas chromosome dynamics increase during sleep. Thus, regulation of the expression of specific genes by chromosome dynamics should be explored. Alternatively, we propose that increased chromosome dynamics enhance the efficiency of DSB elimination during sleep. Notably, although chromosome mobility increases following induction of DSBs, the increase appears to require a threshold level of DNA damage in yeast⁵⁵. In agreement with that, we show that continuous wakefulness inhibits chromosome dynamics, thus preventing the efficient repair of DSBs. We propose that at a given threshold level of DNA damage, sleep is triggered in order to induce chromosome dynamics, which enable the cell to balance between DNA damage and repair (Fig. 6a). Inhibition of a sleep-dependent increase in chromosome dynamics, as demonstrated in the *Lap2β*-overexpressing neurons, can lead to accumulation of DSBs and potentially to cell death. This mechanism can perhaps explain why prolonged sleep deprivation can be lethal⁶, and why aging and neurodegenerative disorders are associated with both abnormal sleep⁵⁶ and increased mutations in the genome of human neurons⁵⁷.

Sleep is typically monitored at the network and whole-organism levels. However, by overcoming a technology barrier, this work determined the effect of sleep on the physiology of single neurons in the context of a live organism. At the cellular level, our results show that a single DNA damaged neuron, but not an endothelial or Schwann cell, requires relatively long periods of sleep in order to increase chromosome dynamics and eliminate the accumulation of DSBs. Indeed, in mammalian cells and embryonic zebrafish cells, clearance of γ H2AX-stained foci typically takes several hours^{58–60}. These nuclear processes are not efficient during prolonged wakefulness, possibly because all cell resources and energy are involved in neuronal function⁶¹. In non-neuronal cell types, such as endothelial and Schwann cells, repair of DSBs may occur in a cell-autonomous manner, which does not affect the behavior of the whole organism. The molecular mechanisms that regulate chromosome dynamics in neurons during sleep and wake require further investigation. *Lap2β* and

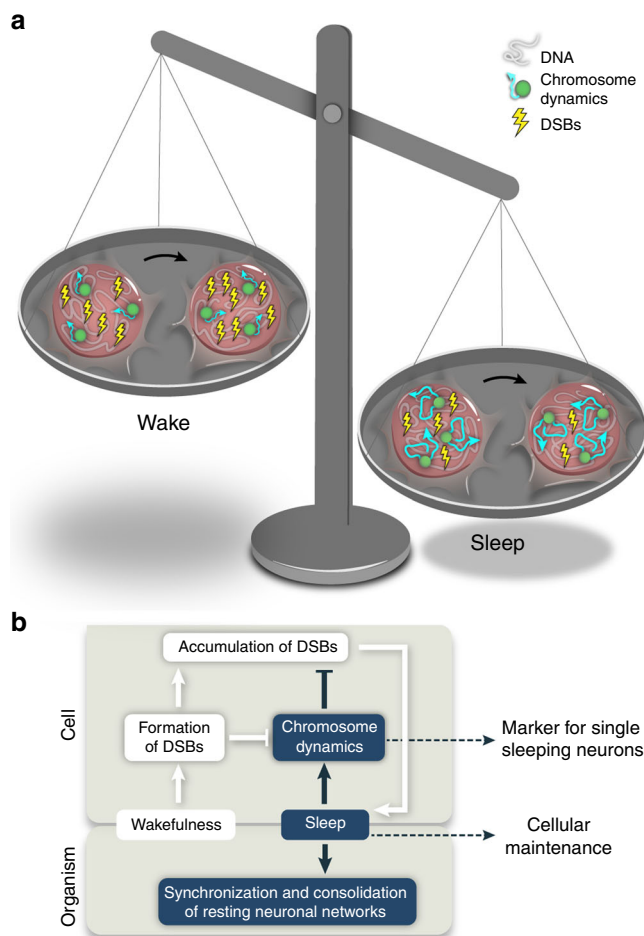


Fig. 6 A proposed function for sleep. **a** During wakefulness, chromosome dynamics are low and the number of DSBs is accumulated in neurons. The beneficial role of sleep is to increase the chromosome dynamics that are essential for the efficient reduction of the number of DSBs in single neurons. **b** DSBs are increased in the nucleus during wakefulness and are formed by intrinsic and extrinsic factors, such as neuronal activity, irradiation, and oxidative stress, when chromosome dynamics are low. At a given threshold, accumulations of DSBs in multiple neuronal networks can trigger sleep, which increases chromosome dynamics that are necessary for the reduction of DNA damage. This mechanism suggests that chromosome dynamics can define single sleeping neurons, and that one of the functions of sleep is nuclear maintenance

lamin A are two potential regulators³⁸; however, the involvement of other factors, such as proteins of the linker of the nucleoskeleton and cytoskeleton (LINC) complex²⁶, cannot be excluded.

At the whole-organism level, an important question is how wake and sleep states affect these cellular processes. We propose that sleep behavior synchronizes and consolidates local sleep in neuronal networks in order to perform essential nuclear maintenance that requires prolonged periods of reduced body movement and responsiveness to external stimuli (Fig. 6b). This is essential because desynchronized networks, where individual neurons reach the rest threshold at various time points, would have disabled the behavioral performance of the animals. Nevertheless, this explanation may not settle with the relatively high global brain activity during sleep that is only slightly lower than during wakefulness in zebrafish⁶². Likewise, in mammals, based on EEG measurements in the cortex, global activity during rapid eye movement (REM) sleep is almost similar to the activity during wakefulness⁶³. Yet, these studies and experimental

approaches focused on average neuronal activity across large brain regions, such as the cortex, while here, we determined the effect of sleep on single neurons, and can differentiate single wake- versus sleep-active neurons. Similarly, in mice, micro-endoscopic calcium imaging of single cells in the dorsal pons showed that wake-active GABAergic neurons are significantly more active during wakefulness than REM and non-rapid eye movement (NREM) sleep⁶⁴. In the zebrafish rhombencephalon, we identified mainly wake-active neurons, suggesting that, at least in the hindbrain but also likely in additional deep brain regions, neurons reduce their activity during sleep. Since, to date, different sleep stages were not detected in fish, future works in mammals are expected to enhance understanding of the correlation between EEG, neuronal activity, and chromosome dynamics in specific neuronal populations during wakefulness, REM, and NREM sleep.

What is the conserved function of sleep? How is it regulated? And how can sleep be defined at the cellular level? Studying sleep across phylogeny can provide key insights into these fundamental questions⁵⁰. Using non-mammalian models, several sleep genes were identified^{1,65}, and sleep-dependent structural synaptic plasticity was visualized in worms, flies, and zebrafish^{66–68}. However, conserved functions and cellular markers were not yet identified. We suggest that in zebrafish, sleep is beneficial to the brain because single neurons can increase chromosome dynamics and perform nuclear maintenance during a consolidated offline period. Future studies on additional vertebrate and invertebrate multicellular animals, ranging from cnidarians to mammals, can establish chromosome dynamics as an evolutionarily conserved cellular sleep marker. This marker may be used to define sleeping single neurons in a live mounted animal even under the microscope, where behavioral criteria are insufficient. Altogether, we postulate that sleep behavior has evolved in order to regulate rest bouts of functionally linked single neurons, thus enabling coordinated nuclear maintenance.

Methods

Zebrafish husbandry and transgenic lines. Adult zebrafish (male and female) were raised and maintained in fully automated zebrafish housing systems (Aqua-zone, Israel; temperature 28 ± 0.5 °C, pH 7.0, conductivity 500 μ S) under 14 h light/10 h dark cycles, and fed twice a day. Embryos were produced by natural spawning and raised in egg-water containing methylene blue (0.3 ppm) in a light-controlled incubator at 28 ± 0.5 °C and under 14 h light/10 h dark cycle. All experiments were done at the larval stages and specific age is indicated at the manuscript. The transgenic lines *tg(uas:EGFP-Terfa)* and *tg(uas:RCaMP1b)* were generated using the Tol2 system⁶⁹. The transgenic lines *tg(mbp:EGFP)*, *tg(HuC:Gal4)*, *tg(fli:Gal4)* and *tg(fli:EGFP)*, as well as *tg(HuC:GCaMP5)* were kindly provided by Cheol-Hee Kim (Chungnam National University Daejeon, Korea), Bettina Schmid (Ludwig Maximilian University of Munich, Germany), Karina Yaniv (Weizmann Institute of Science, Israel), and German Sumbre (Institute de Biologie-Ecole Normale Supérieure, France), respectively. The *aanat2-/-* mutant was kindly provided by David Prober (California Institute of Technology, CA, USA). All animal protocols were reviewed and approved by the Bar-Ilan University Bioethics Committee.

DNA constructs. In order to prepare constructs of chromosome markers, the coding sequences of *terfa* (NM_173243.2) and *cenpa* (NM_001164240.1) were amplified using the following primers: *Terfa*: 5'-ccaaccgggtatgagcgacaaacccctgc-3' and 5'-ccaatcgatcagaccattctgagcttgac-3'; *Cenpa*: 5'-ccaaccgggtatgagcctccatcatcg-3' and 5'-ccaatcgatcagaccattctgagcttgac-3'. The EGFP coding sequence was amplified with 5'-accgaattccaccatggctccaagaagaagcgtaaaggtatggtgagcaagggcgaggagc-3' and 5'-ccaaccgggtatgagcctccatcg-3' primers, the forward primer includes *nls* sequence (underlined). Triple ligation of *EcoRI/ClaI*-digested *pT2-uas:MCS* vector, *EcoRI/AgeI*-digested *egfp*, and *AgeI/ClaI*-digested *terfa* or *AgeI/ClaI*-digested *cenpa* were performed. *pT2-uas:dsRED-TRF1* was generated by amplifying dsRED-TRF1 flanked by *EcoRI/ClaI* from *cmv:dsRED-TRF1* vector (primers: 5'-accgaattccagacttgcctctccgag-3' and 5'-ccaatcgatcagaccattctgagcttgagga-3'), and cloning into *EcoRI/ClaI*-digested *pT2-uas:MCS* vector.

The human TRF1 DNA binding site contains three helices located at the C-terminus of the protein⁷⁰. BLAST analysis of the human TRF1 and zebrafish TRF1 revealed homology (68%) of these motifs. To delete the DNA binding site of *Terfa*, *pT2-uas:EGFP-Terfa del* construct was generated. The *pT2-uas:EGFP-Terfa* construct was amplified using the primers 5'-ggtgactcttttagctggagctgtagaagt-3' and 5'-tgaatcgatgatccagacatgataaga-3', and ligated using T4-ligase (NEB, Ipswich,

MA, USA), which resulted in the deletion of 162 bp in the C-terminus and truncated protein.

In order to prepare the *pT2-mbp:Gal4* construct, approximately 1.9 Kb of the *mbp* promoter (AY860977) was amplified using the primers 5'-ccggggcccaataacaatccaactc-3' and 5'-ccgaccggtgtatgctcttccgctca-3'. The PCR product was digested with *Apal* and *AgeI* restriction enzymes and cloned into *Apal*- and *AgeI*-digested *pT2-hcrt:Gal4* vector replacing the *hcrt* promoter.

In order to prepare the *pT2-uas:RCaMP1b* construct, *RCaMP1b* coding sequence was amplified from *pGP-CMV-NES-jRCaMP1b* (gift from Douglas Kim, Addgene plasmid # 63136)⁷¹, using the 5'-ctcagatctgccaccatgctgcaga-3' and 5'-ttactcggagcggccgctactctgctgc-3' primers. The PCR product was digested with *BglIII* and *XhoI* restriction enzymes and cloned into *BglIII* and *XhoI* digested *pT2-uas:MCS* vector. The *uas:ChR2-YFP* construct was kindly provided by Prof. Philippe Mourrain (Stanford University, USA).

In order to prepare the *pT2-uas:Lap2 β -EGFP* construct, the coding sequences of *lap2 β* (NM_001141787.1) were amplified using the primers 5'-acacgaattccaccatggctccaagaagaagcgtaaaggtatggtgagcaagggcgaggagc-3' and 5'-gttgaaattctgctgctgactgctcactctgctgctc-3'; the forward primer includes the *nls* sequence (underlined). The PCR product was digested by *EcoRI* restriction enzyme and cloned into *EcoRI*-digested *pT2-uas:EGFP* vector.

Imaging. All imaging experiments were conducted on 6–7 dpf larvae. Larvae were mounted with low-melting-point agarose 2.0%, and paralyzed in 0.3 mg/ml pancuronium bromide (P1918, Sigma-Aldrich, St. Louis, MO, USA). Imaging was performed using a Zeiss LSM710 upright confocal/two-photon microscope (Zeiss, Oberkochen, Germany) with $\times 63$, 1.0 NA objective. In order to standardize the optimal conditions for single chromosome imaging, we imaged the motion of single chromosomes using either 2-photon or confocal microscopes. Using either microscope, we observed changes in chromosome dynamics during day and night (2-photon: day— 0.013 ± 0.002 , night— 0.025 ± 0.01 ; confocal: day— 0.009 ± 0.002 , night— 0.027 ± 0.008 ; $n = 5$ Te neurons for each group). Imaging chromosome dynamics using Mai-Tai 2-photon laser (Spectra-Physics, Santa Clara, CA, USA), tuned to 920 nm excitation wavelength, resulted in relatively low signal-to-noise ratio. In contrast, imaging of chromosomes using the confocal microscope equipped with argon laser (488 nm) resulted in an efficient signal-to-noise ratio. This is because high-magnification confocal imaging capture larger focal plan that limits loss of particle trajectories in the *z*-axis. Therefore, in chromosome-dynamic experiments, we used a confocal microscope with the following parameters: image resolution of 256×256 , 50 cycles of 30 planes, speed of 242.04 ms per plane. One plane size was typically $16.8 \times 16.8 \times 1.3$ μ m, with intervals of 0.3 μ m between planes in all Z stacks.

In simultaneous confocal imaging of RCaMP1b and EGFP-Terfa (lasers: argon 488 nm, DPSS 561 nm), the following parameters were used: image resolution of 256×256 , scanning time of 8 min at 4.13 Hz on 16.8×16.8 μ m single plane. In *HuC*-driven GCaMP5 imaging, 6 dpf *tg(HuC:GCaMP5)* larvae were mounted, and GCaMP5 signal was monitored using a Mai-Tai 2-photon laser, tuned to 920 nm, with a $\times 20$ 1.0 NA objective. Scanning was performed at a single plane for 20 min at 4.13 Hz on 140×140 μ m in Te and SC neurons, and 170×170 μ m in Rh neurons.

Transient expression assays. Transient expression assays of the DNA constructs *pT2-uas:EGFP-Terfa-del*, *pT2-uas:dsRED-TRF1*, *pT2-uas:EGFP-Cenpa*, *uas:ChR2-YFP*, *pT2-uas:Lap2 β -EGFP*, and *pT2-mbp:Gal4* were performed by microinjection of approximately 2 nl plasmid into one-cell-stage embryos, at a concentration of 30 ng/ μ l each, using a micromanipulator and PV830 Pneumatic PicoPump (World Precision Instruments, Sarasota, FL). Imaging of all transient experiments was performed in 6 dpf larvae.

Optogenetic experiments. The expression vectors *pT2-uas:dsRED-TRF1* and *pT2-uas:ChR2-YFP* were co-injected into one-cell-stage *tg(HuC:Gal4)* embryos, and positive embryos were raised under 14 h light/10 h dark cycles. At 6 dpf (ZT4), dsRED-TRF1- or dsRED-TRF1+ChR2-YFP-positive neurons were imaged for 10 min with DPSS laser (561 nm). Then, we stimulated the neurons ten times with blue light pulses in 1-s intervals. Following the stimulation, imaging of the same individual neurons was repeated using both DPSS (561 nm) and argon (488 nm) lasers.

Melatonin experiments. Individual 6 dpf *tg(HuC:Gal4)/tg(uas:EGFP-Terfa)* live larvae were treated with either 10 μ M melatonin (M5250, Sigma-Aldrich, St. Louis, MO, USA) or 0.7% EtOH during daytime. Sleep behavior and chromosome dynamics were monitored in Rh neurons of the same larvae before and during treatment with each compound.

BAPTA-AM experiments. Individual 6 dpf *tg(HuC:Gal4)/tg(uas:EGFP-Terfa)* and *tg(HuC:GCaMP5)* live larvae were treated with either 5 mM BAPTA-AM (A1076, Sigma-Aldrich, St. Louis, MO, USA) or 0.1% DMSO diluted in embryo water for 4 h during the night (ZT19–23). During the 4th hour of treatment, chromosome dynamics and neuronal activity were monitored in Rh neurons.

Etoposide experiments. 6 dpf *tg(HuC:Gal4)/tg(uas:EGFP-Terfa)* larvae were treated for 2 h with either 10 μ M etoposide (E1383, Sigma-Aldrich, St. Louis, MO, USA) or 0.01% DMSO diluted in embryo water during day or night. Following treatment, the compound was removed, and the larvae recovered in fresh water. Three parameters were monitored: number of DSBs, chromosome dynamics, and sleep behavior. To quantify the number of DSBs and chromosome dynamics in Rh neurons, larvae were either fixed (for immunohistochemistry) or live-imaged, respectively, following the compound treatment and during the recovery period. In behavioral assays, sleep was monitored as described below.

Behavioral assays. In order to monitor sleep, larvae were individually placed in 48-well plates containing either embryo water, melatonin, ETO, EtOH, or DMSO compound. Larva-containing plates were placed in the Noldus DanioVision tracking system (Noldus Information Technology, Wageningen, Netherlands) under either light or dark. Live video-tracking were conducted using the EthoVision XT 12 software (Noldus Information Technology, Wageningen, Netherlands) with the following parameters for detection: dynamic subtraction, subject is darker than background, dark contrast 16–60, current frame weight 1, subject size of minimum 1 pixel and maximum 125,000 pixels, subject contour turned off, video sample rate of 12.5 frames per second, and no pixel smoothing. Data analyses of sleep time were performed according to the threshold parameters: distance, 0.3 cm; time, stop velocity 0.59 cm/s, start velocity 0.6 cm/s⁴⁰. SD was performed on freely swimming larvae in Petri dishes by 4 h of gentle, random, and unsynchronized manual, mechanical tapping¹¹. Sleep was monitored continuously prior to and 1 h following SD.

Immunohistochemistry assays. Larvae were fixed for 2 h in 4% paraformaldehyde (PFA) in PBS at 4 °C, and washed in PBS + 0.5% Triton. The larvae were then blocked with 10% fetal bovine serum diluted in PBS for 1 h at room temperature. After blocking, the larvae were incubated in primary antibody: rabbit anti-EGFP (SC-8334, Santa Cruz Biotechnology, Santa Cruz, CA), 1:250 dilution; mouse anti- γ H2AX (GTX127342, GeneTex), 1:100 dilution, in blocking buffer overnight at 4 °C. On the following day, larvae were washed in PBS + 0.5% Triton and blocked for 1 h. Anti-GFP was detected with a donkey polyclonal secondary anti-rabbit IgG H&L (Alexa Fluor® 488, 2 mg/ml, ab150061, Abcam), and anti- γ H2AX was detected with donkey anti-mouse IgG H&L (Alexa Fluor® 594) (2 mg/ml, ab150064, Abcam), in blocking buffer overnight at 4 °C. Next, larvae were washed in PBS + 0.5% Triton, fixed for 30 min in 4% PFA in PBS, and washed in PBS + 0.5% Triton.

Data analysis. 3D SPT analysis of a time-lapse image sequence was performed in two stages. First, images were analyzed using Imaris software (Bitplane AG, Zurich, Switzerland), and punctum coordinates were located in each frame using the following parameters: detected ellipsoids with XY diameter of 0.3–0.6 μ m and Z diameter of 1.3 μ m, “quality” filter type to detect as much puncta as possible, and the “autoregressive motion” algorithm, with maximum distance of 1.25 μ m without filling gaps. We verified that there was no concatenation between different puncta, and only punctum trajectories that were continuously trackable during the entire imaging session were quantified. In cases where the entire nucleus, and consequently all chromosomes, rotated significantly in a similar direction, the cells were excluded from the analysis. Then, only a nucleus with at least four reliable tracks was analyzed using custom-made MATLAB software (Mathworks, Natick, MA, USA) for nucleus drift and rotation correction³⁸. In single-plane imaging, analysis was performed in the 1st minute in order limit loss of punctum trajectory in the z-axis.

In calcium imaging analysis (RCaMP1b and GCaMP5), imaging movies were registered to remove drifts using the Template Matching plugin in ImageJ. Then, using the custom-made MATLAB (Mathworks, Natick, MA, USA) programs FindROI and ProcessCalciumData⁷², regions of interest (ROI) were selected, and DeltaFoF and raster plot were determined.

To quantify the number of DSBs, snapshot images of 18 \times 18 μ m were acquired and the number of γ H2AX foci per single cell (~15 cells per image) was counted manually using Cell Counter plugin in ImageJ.

Statistical information. All imaging experiments were performed independently at least three times, whereas at least three larvae were imaged in each independent imaging experiment. In all experiments, larvae were selected randomly. Number of larvae, cells or chromosomes, statistical tests and *P* values are stated in each figure legend. Differences between two categorical groups (ctrl/SD and day/night/subjective day, EtOH/melatonin and pre-/post-treatment, day/night and *aanat2* +/-/*aanat2* -/- or day/night and *Lap2 β* +/-/*Lap2 β* -/-) on continuous variables (chromosome dynamics, sleep, or γ H2AX foci number) were determined by two-way ANOVA using Statistica software (TIBCO). Differences between more than two groups were determined using one-way ANOVA using Statistica software (TIBCO). Differences between two groups were determined by two-tailed *t*-test: two samples assuming unequal variance using Analysis ToolPac in Excel. Changes between paired samples in the optogenetic experiments were determined by two-tailed *t*-test: paired two samples for means using Analysis ToolPac in Excel. Chromosome dynamics and neuronal activity correlation were determined by Pearson correlation coefficient using the social science statistics calculator.

Reporting summary. Further information on experimental design is available in the Nature Research Reporting Summary linked to this article.

Data availability

The data that support the findings of this study are available from the corresponding author upon request.

Received: 15 August 2018 Accepted: 30 January 2019

Published online: 05 March 2019

References

- Levitas-Djerbi, T. & Appelbaum, L. Modeling sleep and neuropsychiatric disorders in zebrafish. *Curr. Opin. Neurobiol.* **44**, 89–93 (2017).
- Trojanowski, N. F. & Raizen, D. M. Call it worm sleep. *Trends Neurosci.* **39**, 54–62 (2016).
- Nath, R. D. et al. The jellyfish *Cassiopea* exhibits a sleep-like state. *Curr. Biol.* **27**, 2984–2990 (2017).
- Zimmerman, J. E., Naidoo, N., Raizen, D. M. & Pack, A. I. Conservation of sleep: insights from non-mammalian model systems. *Trends Neurosci.* **31**, 371–376 (2008).
- Sehgal, A. & Mignot, E. Genetics of sleep and sleep disorders. *Cell* **146**, 194–207 (2011).
- Krause, A. J. et al. The sleep-deprived human brain. *Nat. Rev. Neurosci.* **18**, 404–418 (2017).
- Eban-Rothschild, A., Appelbaum, L. & de Lecea, L. Neuronal mechanisms for sleep/wake regulation and modulatory drive. *Neuropsychopharmacology* **43**, 937–952 (2017).
- Tononi, G. & Cirelli, C. Sleep function and synaptic homeostasis. *Sleep Med. Rev.* **10**, 49–62 (2006).
- Mackiewicz, M. et al. Macromolecule biosynthesis: a key function of sleep. *Physiol. Genomics* **31**, 441–457 (2007).
- Scharf, M. T., Naidoo, N., Zimmerman, J. E. & Pack, A. I. The energy hypothesis of sleep revisited. *Prog. Neurobiol.* **86**, 264–280 (2008).
- Appelbaum, L. et al. Circadian and homeostatic regulation of structural synaptic plasticity in hypocretin neurons. *Neuron* **68**, 87–98 (2010).
- Xie, L. et al. Sleep drives metabolite clearance from the adult brain. *Science* **342**, 373–377 (2013).
- Allada, R. & Siegel, J. M. Unearthing the phylogenetic roots of sleep. *Curr. Biol.* **18**, R670–R679 (2008).
- Zhdanova, I. V., Wang, S. Y., Leclair, O. U. & Danilova, N. P. Melatonin promotes sleep-like state in zebrafish. *Brain Res.* **903**, 263–268 (2001).
- Prober, D. A., Rihel, J., Onah, A. A., Sung, R.-J. & Schier, A. F. Hypocretin/orexin overexpression induces an insomnia-like phenotype in zebrafish. *J. Neurosci.* **26**, 13400–13410 (2006).
- Yokogawa, T. et al. Characterization of sleep in zebrafish and insomnia in hypocretin receptor mutants. *PLoS Biol.* **5**, e277 (2007).
- Saper, C. B. & Fuller, P. M. Wake–sleep circuitry: an overview. *Curr. Opin. Neurobiol.* **44**, 186–192 (2017).
- Rattenborg, N. C., Amlaner, C. J. & Lima, S. L. Behavioral, neurophysiological and evolutionary perspectives on unihemispheric sleep. *Neurosci. Biobehav. Rev.* **24**, 817–842 (2000).
- Vyazovskiy, V. V. & Harris, K. D. Sleep and the single neuron: the role of global slow oscillations in individual cell rest. *Nat. Rev. Neurosci.* **14**, 443–451 (2013).
- Cirelli, C. Cellular consequences of sleep deprivation in the brain. *Sleep Med. Rev.* **10**, 307–321 (2006).
- Allebrandt, K. V. et al. Identifying pathways modulating sleep duration: from genomics to transcriptomics. *Sci. Rep.* **7**, 4555 (2017).
- Thimgan, M. S., Duntley, S. P. & Shaw, P. J. Changes in gene expression with sleep. *J. Clin. Sleep Med.* **7**, S26–S27 (2011).
- Hauer, M. H. & Gasser, S. M. Chromatin and nucleosome dynamics in DNA damage and repair. *Genes Dev.* **31**, 2204–2221 (2017).
- Soutoglou, E. & Misteli, T. Mobility and immobility of chromatin in transcription and genome stability. *Curr. Opin. Genet. Dev.* **17**, 435–442 (2007).
- Christophorou, N. et al. Microtubule-driven nuclear rotations promote meiotic chromosome dynamics. *Nat. Cell Biol.* **17**, 1388–1400 (2015).
- Chang, W., Worman, H. J. & Gundersen, G. G. Accessorizing and anchoring the LINC complex for multifunctionality. *J. Cell Biol.* **208**, 11–22 (2015).
- Shibuya, H., Ishiguro, K. & Watanabe, Y. The TRF1-binding protein TERB1 promotes chromosome movement and telomere rigidity in meiosis. *Nat. Cell Biol.* **16**, 145–156 (2014).
- Takizawa, T. & Meshorer, E. Chromatin and nuclear architecture in the nervous system. *Trends Neurosci.* **31**, 343–352 (2008).

29. Koike, N. et al. Transcriptional architecture and chromatin landscape of the core circadian clock in mammals. *Science* **338**, 349–354 (2012).
30. Hill, A. J., Mansfield, R., Lopez, J. M. N. G., Raizen, D. M. & Van Buskirk, C. Cellular stress induces a protective sleep-like state in *C. elegans*. *Curr. Biol.* **24**, 2399–2405 (2014).
31. Villafuerte, G. et al. Sleep deprivation and oxidative stress in animal models: a systematic review. *Oxid. Med. Cell. Longev.* **2015**, 234952 (2015).
32. Bellesi, M., Bushey, D., Chini, M., Tononi, G. & Cirelli, C. Contribution of sleep to the repair of neuronal DNA double-strand breaks: evidence from flies and mice. *Sci. Rep.* **6**, 36804 (2016).
33. Lieber, M. R. The mechanism of double-strand DNA break repair by the nonhomologous DNA end-joining pathway. *Annu. Rev. Biochem.* **79**, 181–211 (2010).
34. Suberbielle, E. et al. Physiologic brain activity causes DNA double-strand breaks in neurons, with exacerbation by amyloid- β . *Nat. Neurosci.* **16**, 613–621 (2013).
35. Madabhushi, R. et al. Activity-induced DNA breaks govern the expression of neuronal early-response genes. *Cell* **161**, 1592–1605 (2015).
36. Yadav, T., Quivy, J.-P. & Almourzi, G. Chromatin plasticity: a versatile landscape that underlies cell fate and identity. *Science* **361**, 1332–1336 (2018).
37. Bronshtein, I. et al. Exploring chromatin organization mechanisms through its dynamic properties. *Nucleus* **7**, 27–33 (2016).
38. Bronshtein, I. et al. Loss of lamin A function increases chromatin dynamics in the nuclear interior. *Nat. Commun.* **6**, 8044 (2015).
39. Elbaz, I., Foulkes, N. S., Gothilf, Y. & Appelbaum, L. Circadian clocks, rhythmic synaptic plasticity and the sleep–wake cycle in zebrafish. *Front. Neural Circuits* **7**, 9 (2013).
40. Elbaz, I., Yelin-Bekerman, L., Nicenboim, J., Vatine, G. & Appelbaum, L. Genetic ablation of hypocretin neurons alters behavioral state transitions in zebrafish. *J. Neurosci.* **32**, 12961–12972 (2012).
41. Appelbaum, L. et al. Sleep–wake regulation and hypocretin–melatonin interaction in zebrafish. *Proc. Natl Acad. Sci. USA* **106**, 21942–21947 (2009).
42. Gothilf, Y. et al. Zebrafish serotonin N-acetyltransferase-2: marker for development of pineal photoreceptors and circadian clock function. *Endocrinology* **140**, 4895–4903 (1999).
43. Gandhi, A. V., Mosser, E. A., Oikonomou, G. & Prober, D. A. Melatonin is required for the circadian regulation of sleep. *Neuron* **85**, 1193–1199 (2015).
44. Vilenchik, M. M. & Knudson, A. G. Endogenous DNA double-strand breaks: production, fidelity of repair, and induction of cancer. *Proc. Natl. Acad. Sci. USA* **100**, 12871–12876 (2003).
45. Smart, D. J. et al. Assessment of DNA double-strand breaks and gammaH2AX induced by the topoisomerase II poisons etoposide and mitoxantrone. *Mutat. Res.* **641**, 43–47 (2008).
46. Dechat, T., Vlcek, S. & Foisner, R. Review: lamina-associated polypeptide 2 isoforms and related proteins in cell cycle-dependent nuclear structure dynamics. *J. Struct. Biol.* **129**, 335–345 (2000).
47. Schoft, V. K. et al. The lamina-associated polypeptide 2 (LAP2) isoforms beta, gamma and omega of zebrafish: developmental expression and behavior during the cell cycle. *J. Cell Sci.* **116**, 2505–2517 (2003).
48. Ahrens, M. B. et al. Brain-wide neuronal dynamics during motor adaptation in zebrafish. *Nature* **485**, 471–477 (2012).
49. Boyden, E. S., Zhang, F., Bamberg, E., Nagel, G. & Deisseroth, K. Millisecond-timescale, genetically targeted optical control of neural activity. *Nat. Neurosci.* **8**, 1263–1268 (2005).
50. Joiner, W. J. Unraveling the evolutionary determinants of sleep. *Curr. Biol.* **26**, R1073–R1087 (2016).
51. Cirelli, C. & Tononi, G. Is sleep essential? *PLoS Biol.* **6**, e216 (2008).
52. Misteli, T. Higher-order genome organization in human disease. *Cold Spring Harb. Perspect. Biol.* **2**, a000794 (2010).
53. Gu, B. et al. Transcription-coupled changes in nuclear mobility of mammalian cis-regulatory elements. *Science* **359**, 1050–1055 (2018).
54. Bellesi, M., de Vivo, L., Tononi, G. & Cirelli, C. Effects of sleep and wake on astrocytes: clues from molecular and ultrastructural studies. *BMC Biol.* **13**, 66 (2015).
55. Seeber, A., Dion, V. & Gasser, S. M. Checkpoint kinases and the INO80 nucleosome remodeling complex enhance global chromatin mobility in response to DNA damage. *Genes Dev.* **27**, 1999–2008 (2013).
56. Grigg-Damberger, M. M. Sleep in aging and neurodegenerative diseases. *Suppl. Clin. Neurophysiol.* **57**, 508–520 (2004).
57. Lodato, M. A. et al. Aging and neurodegeneration are associated with increased mutations in single human neurons. *Science* **359**, 555–559 (2018).
58. Leatherbarrow, E. L., Harper, J. V., Cucinotta, F. A. & O'Neill, P. Induction and quantification of gamma-H2AX foci following low and high LET-irradiation. *Int. J. Radiat. Biol.* **82**, 111–118 (2006).
59. Shibata, A. et al. Factors determining DNA double-strand break repair pathway choice in G2 phase. *EMBO J.* **30**, 1079–1092 (2011).
60. Pereira, S. et al. Low doses of gamma-irradiation induce an early bystander effect in zebrafish cells which is sufficient to radioprotect cells. *PLoS ONE* **9**, e92974 (2014).
61. Shetty, P. K., Galeffi, F. & Turner, D. A. Cellular links between neuronal activity and energy homeostasis. *Front. Pharmacol.* **3**, 43 (2012).
62. Lee, D. A. et al. Genetic and neuronal regulation of sleep by neuropeptide VF. *eLife* **6**, e25727 (2017).
63. Brown, R. E., Basheer, R., McKenna, J. T., Strecker, R. E. & McCarley, R. W. Control of sleep and wakefulness. *Physiol. Rev.* **92**, 1087–1187 (2012).
64. Cox, J., Pinto, L. & Dan, Y. Calcium imaging of sleep–wake related neuronal activity in the dorsal pons. *Nat. Commun.* **7**, 10763 (2016).
65. Raizen, D. M. & Zimmerman, J. E. Non-mammalian genetic model systems in sleep research. *Sleep Med. Clin.* **6**, 131–139 (2011).
66. Wang, G., Grone, B., Colas, D., Appelbaum, L. & Mourrain, P. Synaptic plasticity in sleep: learning, homeostasis and disease. *Trends Neurosci.* **34**, 452–463 (2011).
67. Dabbish, N. S. & Raizen, D. M. GABAergic synaptic plasticity during a developmentally regulated sleep-like state in *C. elegans*. *J. Neurosci.* **31**, 15932–15943 (2011).
68. Donlea, J. M., Ramanan, N. & Shaw, P. J. Use-dependent plasticity in clock neurons regulates sleep need in *Drosophila*. *Science* **324**, 105–108 (2009).
69. Kawakami, K. et al. A transposon-mediated gene trap approach identifies developmentally regulated genes in zebrafish. *Dev. Cell* **7**, 133–144 (2004).
70. Hanaoka, S., Nagadoi, A. & Nishimura, Y. Comparison between TRF2 and TRF1 of their telomeric DNA-bound structures and DNA-binding activities. *Protein Sci.* **14**, 119–130 (2005).
71. Dana, H. et al. Sensitive red protein calcium indicators for imaging neural activity. *eLife* **5**, e12727 (2016).
72. Romano, S. A. et al. An integrated calcium imaging processing toolbox for the analysis of neuronal population dynamics. *PLoS Comput. Biol.* **13**, e1005526 (2017).

Acknowledgements

The authors thank the members of the Appelbaum lab for technical assistance, Noa Alon for assistance in designing the schematic illustrations, and Luis de Lecea, David Klein, German Sumbre, Eran Meshorer, and Ofer Yizhar for helpful discussions and comments. The authors also thank Ms. Sharon Victor for assistance in editing the manuscript. This work was supported by the Israel Science Foundation (Grant no. 690/15 to L.A.) and by the US–Israel Binational Science Foundation (BSF, Grant no. 2017105 to L.A.).

Author contributions

D.Z. and L.A. conceived and designed the experiments. D.Z. performed molecular, imaging, and behavioral experiments. T.L.-G. performed immunohistochemistry experiments. D.Z. and L.A. analyzed data. Y.G. and I.B. analyzed chromosome dynamic experiments and supplied reagents. D.Z. and L.A. prepared the figures and wrote the paper, with feedback from all authors.

Additional information

Supplementary Information accompanies this paper at <https://doi.org/10.1038/s41467-019-08806-w>.

Competing interests: The authors declare no competing interests.

Reprints and permission information is available online at <http://npg.nature.com/reprintsandpermissions/>

Journal peer review information: *Nature Communications* thanks Roberto Peeza and other anonymous reviewer(s) for their contribution to the peer review of this work.

Publisher's note: Springer Nature remains neutral with regard to jurisdictional claims in published maps and institutional affiliations.



Open Access This article is licensed under a Creative Commons Attribution 4.0 International License, which permits use, sharing, adaptation, distribution and reproduction in any medium or format, as long as you give appropriate credit to the original author(s) and the source, provide a link to the Creative Commons license, and indicate if changes were made. The images or other third party material in this article are included in the article's Creative Commons license, unless indicated otherwise in a credit line to the material. If material is not included in the article's Creative Commons license and your intended use is not permitted by statutory regulation or exceeds the permitted use, you will need to obtain permission directly from the copyright holder. To view a copy of this license, visit <http://creativecommons.org/licenses/by/4.0/>.

© The Author(s) 2019